Anisotropic magneto-optical absorption and linear dichroism in two-dimensional semi-Dirac electron systems

Xiaoying Zhou,* Wang Chen, and Xianzhe Zhu

Department of Physics, Key Laboratory for Low-Dimensional Structures and Quantum Manipulation (Ministry of Education), Hunan Normal University, Changsha 410081, China

(Received 16 September 2021; accepted 22 November 2021; published 2 December 2021)

We present a theoretical study on the Landau levels (LLs) and magneto-optical absorption of a two-dimensional semi-Dirac electron system under a perpendicular magnetic field. Based on an effective $\boldsymbol{k}\cdot\mathbf{p}$ Hamiltonian, we find that the LLs are proportional to the two-thirds power law of the magnetic field and level index, which can be understood as a hybridization of the LL of Schrödinger and Dirac electrons with new features. With the help of the Kubo formula, we find the selection rule for interband (intraband) magneto-optical transition is anisotropic (isotropic). Specifically, the selection rules for interband magneto-optical transitions are $\Delta n = 0, \pm 2$ ($\pm 2, \pm 4$) for linearly polarized light along the linear (parabolic) dispersion direction, while the selection rules for the intraband transition are $\Delta n = \pm 1, \pm 3$ regardless of the polarization direction of the light. Further, the magneto-optical conductivity for interband (intraband) transition excited by linearly polarized light along the linear dispersion direction is two (one) orders of magnitude larger than that along the parabolic dispersion direction. This anisotropic magneto-optical absorption spectrum clearly reflects the structure of the LLs, and results in a strong linear dichroism. Importantly, a perfect linear dichroism with magnetic-field tunable wavelength can be achieved by using the interband transition between the two lowest LLs, i.e., from E_{v0} to E_{c0}. Our results shed light on the magneto-optical property of the two-dimensional semi-Dirac electron systems and pave the way to design magnetically controlled optical devices.

DOI: 10.1103/PhysRevB.104.235403

I. INTRODUCTION

In the past decade, the study on the Dirac-Weyl fermions in condensed matter systems has attracted intensive attention on account of both rich physics therein and promising applications [1,2]. The two-dimensional (2D) semi-Dirac material is a new kind of highly anisotropic electron system, of which the low-energy dispersion is linear along one direction and parabolic along the perpendicular direction [3–5]. Owing to the unique dispersion, a semi-Dirac material has the properties of both Dirac materials and conventional semimetals or semiconductors [3–5]. Various systems are predicted to host 2D semi-Dirac electrons such as the anisotropic strain modulated graphene [3,4], the multilayer $(TiO_2)_n/(VO_2)_m$ nanostructures [5–7], and the strained or electric field-modulated few-layer black phosphorus [8–12]. Recently, the semi-Dirac electron has been observed experimentally in potassium-doped and strained few-layer phosphorene [13,14].

Although the low-energy dispersion of a semi-Dirac material is a hybridization of that in Dirac materials and conventional semimetals, it still exhibits unique features which cannot be fully understood by combing the existing results of the two typical materials. Those features include the unusual Landau levels (LLs) [3–5], the optical conductivity [15,16], the anisotropic plasmon [17], the Fano factor in ballistic transport [18], the power-law decay indexes in the quasiparticle interference spectrum [19], and so on. In particular, the LLs of the 2D semi-Dirac electron system are proportional to the two-thirds power law of the magnetic field and level index, i.e., $E_n \propto [(n + 1/2)B]^{2/3}$ [4], which has been verified by the magnetotransport experiment [14]. This is different from the linear dependence on the magnetic field and the level index in conventional semimetals or semiconductors [20,21] and the square root power dependence in pure Dirac materials [22–24]. The LL structure is an important fundamental issue for electron material systems because it dominates the magneto-properties, such as the quantum Hall effect, magneto-optical and magneto-resonance features of the material [20–24]. In turn, magneto-measurement is also a powerful tool to detect the structure of the LLs [21–29]. Further, the band parameters such as the effective masses and the Fermi velocity can be extracted from the measured LL spectrum, which has been successfully applied in graphene [22–26], the surface states of three-dimensional topological insulators [27,28], and 2D black phosphorus [29]. To date, there are already several theoretical works on the LLs of the semi-Dirac electron system [3–5] and also a magneto-transport measurement on it [14]. However, the magneto-optical property of the 2D semi-Dirac electron system still remains elusive.

In this work, we theoretically investigate the LLs and magneto-optical properties of a 2D semi-Dirac electron system under a perpendicular magnetic field. Using the formula given by the Sommerfeld quantization to fit the numerical calculations, we find that the LLs are proportional to the 2/3 power of the magnetic field and the level index, which is

*xiaoyingzhou@hunnu.edu.cn

different from that in the conventional semimetals or semiconductors [20,21] and the massless Dirac materials [22–24]. There is a band gap in the LL spectrum, and the LL spacings decrease with the increase of the level index. With the help of the Kubo formula, we evaluate the longitudinal magneto-optical conductivity as functions of the photon energy. We find the selection rule for interband (intraband) magneto-optical transitions is anisotropic (isotropic). The selection rules for interband transitions are $\Delta n = 0, \pm 2$ ($\pm 2, \pm 4$) for linearly polarized light along the linear (parabolic) dispersion direction, while the selection rules for intraband transitions are $\Delta n = \pm 1, \pm 3$ regardless of the polarization direction of the light. For interband (intraband) transitions, the magneto-optical conductivity excited by the linearly polarized light along the linear dispersion direction is hundreds (dozens) times larger than that along the parabolic dispersion direction. The anisotropic magneto-optical absorption spectrum clearly reflects the LL structure and results in a strong linear dichroism. Importantly, the interband transition between the two lowest-LLs results in a perfect linear dichroism with magnetic field tunable wavelength, which is useful to design magneto-optical devices.

The rest of the paper is organized as follows. In Sec. II, we introduce the calculation of LLs and magneto-optical properties based on the Kubo formula. In Sec. III, we present the numerical results and discussions. Finally, we summarize our results in Sec. IV.

II. LANDAU LEVELS AND MAGNETO-OPTICAL TRANSITIONS

A. Landau levels

The low-energy effective Hamiltonian of a 2D semi-Dirac electron system is [3,8]

$$H = \frac{p_y^2}{2m^*}\sigma_x + v_F p_x \sigma_y, \tag{1}$$

where σ_x and σ_y are the Pauli matrices, $\mathbf{p} = (\hbar k_x, \hbar k_y)$ the momentum, m^* the effective mass, and v_F the Fermi velocity. Typically, in potassium-doped few-layer black phosphorus, the two parameters are [8] $v_F = 3 \times 10^5$ m/s and $m^* = 1.42\, m_0$, where m_0 is the free electron mass. The eigenvalue of Hamiltonian (1) is

$$E_s = s\sqrt{p_y^4/4m^{*2} + v_F^2 p_x^2}, \tag{2}$$

where the sign $s = +/-$ stands for the conduction/valence band. Equation (2) indicates that the low-energy state of a 2D semi-Dirac electron system is highly anisotropic, of which the dispersion is linear (parabolic) in the $k_x(k_y)$-direction. When a perpendicular magnetic field $\mathbf{B} = (0, 0, B)$ is applied, performing the Peierls substitution $\mathbf{p} \to \pi = \mathbf{p} + \mathbf{eA}$, we have the commutator $[\pi_x, \pi_y] = -ieB\hbar$. Hence, the creation and annihilation operators can be defined as

$$\hat{a} = \frac{l_B}{\sqrt{2}\hbar}(\pi_x - i\pi_y), \quad \hat{a}^\dagger = \frac{l_B}{\sqrt{2}\hbar}(\pi_x + i\pi_y), \tag{3}$$

where $l_B = \sqrt{\hbar/eB}$ is the magnetic length. Therefore, Hamiltonian (1) can be rewritten as

$$H = -\frac{\hbar^2}{4m^* l_B^2}(\hat{a}^\dagger - \hat{a})^2\sigma_x + \frac{\hbar v_F}{\sqrt{2}l_B}(\hat{a}^\dagger + \hat{a})\sigma_y. \tag{4}$$

This Hamiltonian cannot be solved analytically because the creation and annihilation operators couple all the LLs together. Fortunately, it can be solved numerically by taking the eigenvectors of the number operator $\hat{n} = \hat{a}^\dagger\hat{a}$ as basis functions. In this basis, the wave function of the system can be written as

$$\psi = \sum_{m=0}^{M} \begin{pmatrix} u_m \\ v_m \end{pmatrix} |m\rangle, \tag{5}$$

where u_m and v_m are the linear superposition coefficients and M is the total number of basis functions. Then, we can diagonalize Hamiltonian (4) numerically in a truncated Hilbert space and obtain the eigenvalues as well as the eigenvectors. In the Landau gauge $\boldsymbol{A} = (-By, 0, 0)$, the basis function $|m\rangle$ is $\langle r|m\rangle = \varphi(x, y) = \frac{e^{ik_x x}}{\sqrt{L_x}}\phi_m(y - y_0)$, where $\phi_m(.)$ is the eigenvector of the one-dimensional harmonic oscillator and $y_0 = k_x l_B^2$ is the cyclotron center.

Another way to obtain the eigenvalues of Hamiltonian (4) is to use a semiclassical argument, e.g., the Sommerfeld quantization [3]. The formula of LL spectrum is given as

$$E_{s,n} = s\alpha_n\left[\frac{\hbar v_F e}{\sqrt{m^*}}\left(n + \frac{1}{2}\right)B\right]^{2/3}, \quad n = 0, 1, 2, 3, \ldots, \tag{6}$$

where α_n depends on the Landau level index n. To determine α_n, we need to fit Eq. (6) with the numerical data. In our work, we find $\alpha_0 = 0.9454$, $\alpha_1 = 1.1668$, and $\alpha_n = 1.1723$ for $n \geqq 2$. At this point, it is interesting to compare the LLs of 2D semi-Dirac electron systems with those of Schrödinger electrons in conventional semi-metal or semiconductors, and Dirac electrons in graphene. The results are summarized as

$$E_n = \begin{cases} \frac{\hbar eB}{m^*}(n + \frac{1}{2}) : \text{Schrödinger electrons}, \\ \mathrm{sgn}(n) v_F\sqrt{2\hbar eB|n|} : \text{Dirac electrons}, \\ \mathrm{sgn}(n)\alpha_n[\sqrt{\frac{\hbar eB}{m^*}} v_F\sqrt{\hbar eB}(|n| + \frac{1}{2})]^{2/3} : \text{semi-Dirac electrons}. \end{cases} \tag{7}$$

Obviously, the LLs of the three kinds of 2D electron gas are different from each other. Further, the LL spacings for $n \geqq 2$ are

$$\begin{aligned} \Delta E_n &= E_{s,n+1} - E_{s,n} \\ &= \frac{2(n+1)\epsilon_0}{\left(n + \frac{3}{2}\right)^{4/3} + \left(n + \frac{1}{2}\right)^{4/3} + \left(n + \frac{3}{2}\right)^{2/3}\left(n + \frac{1}{2}\right)^{2/3}}, \end{aligned} \tag{8}$$

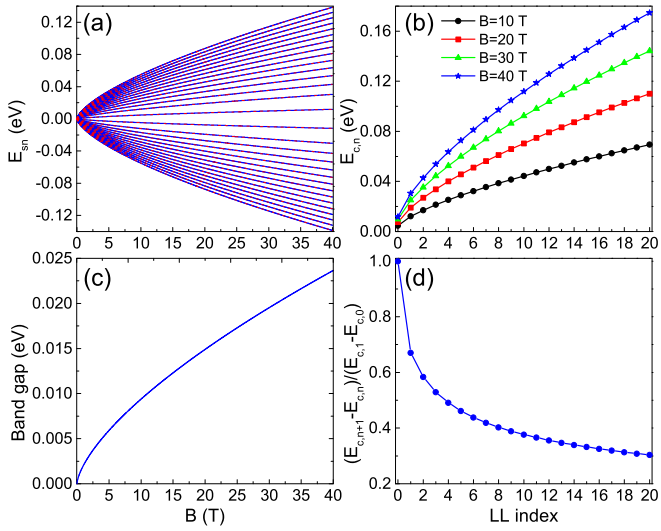

FIG. 1. (a) LLs as a function of magnetic field for the lowest 15 subbands, where the blue solid (red dashed) lines indicate the numerical (analytical) results. (b) LLs in the conduction band varying with level index under different magnetic fields. (c) Band gap of the LL spectrum versus magnetic field. (d) LL spacings in the conduction band (blue line) in unit of the first one ($E_{c,1} - E_{c,0}$) as a function of level index under magnetic field $B = 30$ T.

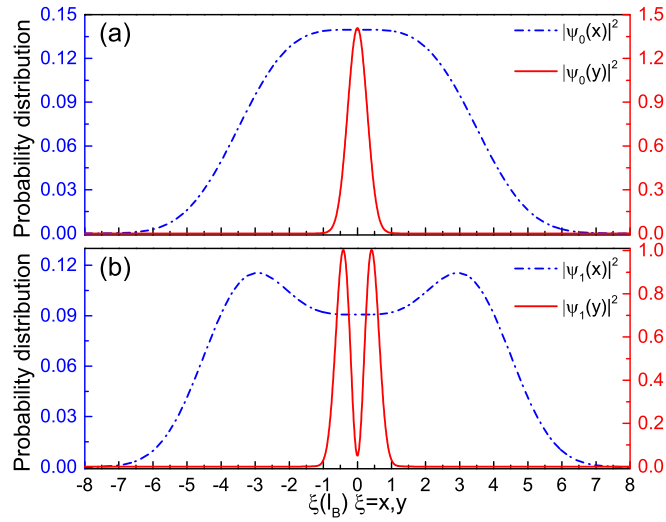

FIG. 2. [(a), (b)] The spatial probability distributions of the first/second LLs in the conduction when choose different gauges for the vector potential **A**. The blue/red lines represent the probability distribution along the x/y-direction.

where $\epsilon_0 = \alpha_2(\hbar v_F eB/\sqrt{m^*})^{2/3}$. Meanwhile, it is also interesting to compare the cyclotron resonance energies at the quasiclassical limit for three kinds of two-dimensional electron gas, which are summarized as

$$\hbar\omega_c = \begin{cases} \frac{\hbar eB}{m^* c} & \text{: Schrödinger electrons} \\ \frac{\hbar v_F^2 eB}{cE_F} & \text{: Dirac electrons [30,31]} \\ \frac{\hbar\Gamma(\frac{3}{4})}{2\Gamma(\frac{5}{4})}\sqrt{\frac{m^* v_F^2}{2E}}\frac{eB}{m^* c} & \text{: emi-Dirac electrons [17].} \end{cases} \tag{9}$$

From Eq. (9), we see that the quasiclassical cyclotron resonance energies all linearly depend on the magnetic field.

Figure 1(a) plots the LLs as a function of the magnetic field for the lowest 15 subbands. From Fig. 1(a), we find that the LLs (the red lines) given by Sommerfeld quantization [see Eq. (6)] perfectly reproduce the numerical results (blue lines) under any magnetic field. This proves that the LLs of the 2D semi-Dirac electron system are proportional to the $2/3$ power law of the magnetic field. Moreover, the LLs also show $2/3$ power-law dependence on the level index under different magnetic fields [see Fig. 1(b)]. This $2/3$ power dependence on the magnetic field and level index is different from that in conventional semimetals or semiconductors [20,21] or Dirac materials [22–24]. Although semi-Dirac electrons are realized in potassium-doped few-layer black phosphorus [13], the LLs are already quite different from those of pristine black phosphorus [32–35], indicating that they have become different electron systems. In contrast to the gapless LLs of Dirac materials [22–24], there is a band gap in the LL spectrum due to the zero-point energy of the harmonic oscillator, which is more similar to that in conventional semiconductors [20,21]. The band gap is $2E_{c,0}$ which increases with the $2/3$ power law of the magnetic field [see Fig. 1(c)]. The stronger the magnetic field, the larger the band gap. Further, Fig. 1(d) shows the LL spacings in the conduction band in unit of the first one ($E_{c,1} - E_{c,0}$) as a function of the level index under magnetic field $B = 30$ T. From Fig. 1(d), we find that the LL spacings decrease with increasing level index, which can also be inferred from Eq. (8). In other words, the higher the level index, the smaller the LL spacing. For the high-level index limitation ($n \to \infty$), the LL spacing vanishes.

Unlike the highly anisotropic dispersion at zero magnetic field [see Eq. (2)], the LLs of a 2D semi-Dirac electron system are independent of the wave vectors and seem to be isotropic. However, the anisotropy of the LLs can be revealed from the wave functions. Figures 2(a) and 2(b) plot the spatial probability distributions in different Landau gauges of the first and second LL, respectively. The probability distributions are calculated by using the finite difference method [36] which is not presented here. As plotted in Fig. 2, we find that the probability distribution exhibits strong anisotropy. It decays much faster along the y-direction (red lines) than that along the x-direction (blue lines). This means that electrons are more localized in the y-direction due to the larger effective mass along this direction. The highly anisotropic probability distribution (wave function) plays an important role in the magneto-optical absorption spectrum of the 2D semi-Dirac electron system as shall be discussed later.

To conclude this subsection, the LL spectrum of a 2D semi-Dirac electron can be understood as a hybridization of that of the Schrödinger and Dirac electron but with new features. In particular, the band gap arising from the zero-point energy is inherited from the Schrödinger electron, while the decreasing LL spacing is inherited from the Dirac electron. However, the $2/3$ power-law dependence on the magnetic field and level index as well as the highly anisotropic wave function are not embedded in the LL spectrum of Schrödinger and Dirac electron systems.

B. Magneto-optical properties

Within the linear response theory, the dynamical conductivity can be written as [37–40]

$$\sigma_{\mu\nu}(\omega) = \frac{\hbar e^2}{iS_0}\sum_{\xi\neq\xi'}\frac{[f(E_\xi)-f(E_{\xi'})]\langle\xi|v_\mu|\xi'\rangle\langle\xi'|v_\nu|\xi\rangle}{(E_\xi-E_{\xi'})(E_\xi-E_{\xi'}+\hbar\omega+i\Gamma_\xi)}, \tag{10}$$

where $\hbar\omega$ is the photon energy, $S_0 = L_xL_y$ the sample area with the size L_x (L_y) in the x (y)-direction, $|\zeta\rangle = |s, n, k_x\rangle$ the wave function expressed in Eq. (5), $f(E_\xi) = [e^{(E_\xi-E_F)/k_BT}+1]^{-1}$ the Fermi-Dirac distribution function with Boltzman constant k_B and temperature T. The sum runs over all states $|\xi\rangle = |s, n, k_x\rangle$ and $|\xi'\rangle = |s', n', k_x'\rangle$ with $\xi\neq\xi'$. Meanwhile, $\Gamma_\xi \propto \sqrt{B}$ accounts for the LL broadening induced by the disorder effects [37,41]. In the simplest approximation, we can assume the broadenings are the same for each LL. The velocity matrix operators $v_{x/y} = \partial H/\partial p_{x/y}$ are

$$v_x = v_F\sigma_y, \quad v_y = -iv_0(\hat{a}^\dagger-\hat{a})\sigma_x, \tag{11}$$

where $v_0 = \hbar/\sqrt{2}l_Bm^*$. It is worth noting that the velocity operators are anisotropic, which will result in a highly anisotropic magneto-optical absorption spectrum. Under moderate magnetic fields, the absorption for linearly polarized light along the x-direction is stronger than that along the y-direction because of $v_F > v_0$. Meanwhile, we note that v_x (v_y) is independent (dependent) on the creation and annihilation operators, which means the magneto-optical transition selection rules may also be anisotropic. By using the wave function in Eq. (5), the transition matrix elements of the velocity matrices are

$$\begin{aligned}
X^{s',s}_{n',n} &= \langle s', n', k_x'|v_x|s, n, k_x\rangle \\
&= \sum_{m',m}^{M} iv_F\big(-u^{n',s'*}_{m'}v^{n,s}_m + v^{n',s'*}_{m'}u^{n,s}_m\big)\delta_{m',m}, \\
Y^{s,s'}_{n,n'} &= \langle s, n, k_x|v_y|s', n', k_x'\rangle \\
&= \sum_{m,m'}^{M} -iv_0\big(u^{n,s*}_m v^{n',s'}_{m'} + v^{n,s*}_m u^{n',s'}_{m'}\big) \\
&\quad\times(-\sqrt{m}\delta_{m',m-1}+\sqrt{m+1}\delta_{m',m+1}).
\end{aligned} \tag{12}$$

By Fermi's golden rule [42,43], the transition rate from the nth LL in the s band to the n'th one in the s' band for linearly polarized light along the x-direction is

$$\begin{aligned}
T_x^{s'n',sn} &= \frac{2\pi}{\hbar}\left(\frac{\hbar}{l_B}\left|X^{s,s'}_{n,n'}\right|\right)^2\delta(E_{s'n'}-E_{sn}\pm\hbar\omega)f(E_{s'n'}) \\
&\quad\times[1-f(E_{sn})],
\end{aligned} \tag{13}$$

while $T_y^{s'n',sn}$ is similar to $T_x^{s'n',sn}$. Hence, the normal of the matrix elements $|X^{s',s}_{n',n}|^2$ and $|Y^{s',s}_{n',n}|^2$ directly determine the magneto-optical transition selection rules. A zero matrix element represents a forbidden transition. Although the transition matrix elements [see Eq. (12)] cannot be obtained analytically, we can still obtain the magneto-optical transition selection rules by numerically checking all the matrix elements of the transition rate one by one. With the velocity matrix elements in Eq. (12), one can evaluate the magneto-optical conductivity for linearly polarized light directly. Substituting Eq. (12) into Eq. (10) and making the replacement $\sum_{k_x}\to g_sS_0/2\pi l_B^2$, where $g_s = 2$ for the spin degeneracy, we obtain the real (absorption) part of the longitudinal magneto-optical conductivity as

$$\frac{\mathrm{Re}\sigma_{\mu\mu}}{\sigma_0} = \sum_{n,n',s,s'}\frac{[f(E_{n',s'})-f(E_{n,s})]\left|\mu^{s',s}_{n',n}\right|^2\Gamma}{(E_{n,s}-E_{n',s'})[(E_{n,s}-E_{n',s'}+\hbar\omega)^2+\Gamma^2]}, \tag{14}$$

where μ=(x, y), $x^{s',s}_{n',n} = \hbar X^{s',s}_{n',n}/l_B$, $y^{s',s}_{n',n} = \hbar Y^{s',s}_{n',n}/l_B$, and $\sigma_0 = 2e^2/h$. Similarly, the expression for the absorption (imaginary) part of the Hall magneto-optical conductivity is

$$\frac{\mathrm{Im}\sigma_{xy}}{\sigma_0} = \sum_{n,n',s,s'}\frac{f(E_{n,s})-f(E_{n',s'})\Gamma\mathrm{Im}\big(x^{s,s'}_{n,n'}y^{s',s}_{n',n}\big)}{(E_{n,s}-E_{n',s'})[(E_{n,s}-E_{n',s'}+\hbar\omega)^2+\Gamma^2]}, \tag{15}$$

where $\mathrm{Im}(x^{s,s'}_{n,n'}y^{s',s}_{n',n})$ determines the transition rate and $x^{s,s'}_{n,n'}y^{s',s}_{n',n} = \frac{\hbar^2}{l_B^2}\langle s, n|v_x|s', n'\rangle\langle s', n'|v_y|s, n\rangle$ is purely imaginary.

III. RESULTS AND DISCUSSION

In this section, we present the numerical results and discussions for the magneto-optical conductivities. Hereafter, unless explicitly specified, the conductivities are all in units of $\sigma_0 = 2e^2/h$, temperature $T = 1$K, Fermi energy $E_F = 0$ for interband transitions, and level broadening $\Gamma = 0.05\sqrt{B}$ in unit of meV.

To understand the magneto-optical absorption spectra, we first examine the interband magneto-optical selection rules determined by the matrix elements of the transition rate. Figures 3(a) and 3(b) plot all the nonzero matrix elements of the transition rate for the interband transition as a function of the photon energy. As shown in Figs. 3(a) and 3(b), the matrix elements $T_x^{vn,cn'}$ ($T_y^{vn,cn'}$) are nonzero only if the level indexes satisfy $|n-n'|$=0,2 ($|n-n'|$ =2,4), which indicates that the interband magneto-optical selection rule for linearly polarized light along the $x(y)$-direction is $\Delta n = 0, \pm2$ ($\pm2, \pm4$), where we defined $\Delta n = n - n'$. Surprisingly, the interband magneto-optical selection rule of the semi-Dirac electron system is anisotropic. This is quite different from the dipole transition ($\Delta n = \pm1$) in conventional semiconductors [44] and Dirac materials [38–40,45,46]. It also differs from the isotropic selection rule in black phosphorus thin film [32,35] in spite of the highly anisotropic dispersion therein. We schematically illustrated the interband magneto-optical selection rules in Fig. 3(c), where the magenta, orange, and purple arrows denote the interband transitions of $\Delta n = 0, \pm2, \pm4$, respectively. Further, in the low photon energy regime, there are well-resolved two-peak structures in the transition rate spectra arising from the two kinds of transitions, i.e., $\Delta n = 0, \pm2$ or $\Delta n = \pm2, \pm4$. However, the two peaks in the transition rate spectra tend to coincide with each other with increasing photon energy and finally merge together in the high photon energy regime [see the purple and orange lines in Fig. 3(a)].

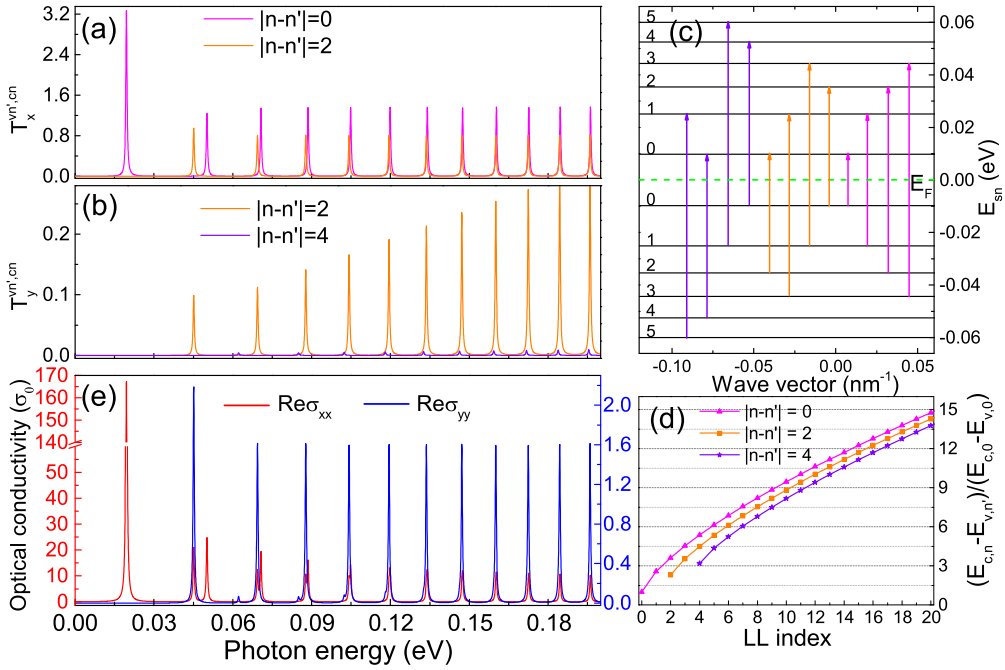

FIG. 3. [(a), (b)] Nonzero elements of the interband transition rate as a function of photon energy for linearly polarized light along the x/y-direction with magnetic field $B = 30$ T. (c) Schematic illustration of the interband magneto-optical transition rules, where the magenta, orange, and purple arrows denote the interband transitions of $\Delta n = |n - n'| = 0, \pm 2, \pm 4$, respectively. (d) The photon energies of the three kinds of interband transitions with $|n - n'| = 0, \pm 2, \pm 4$ in units of the band gap as a function of level index. (e) The real part of the longitudinal magneto-optical conductivity (in units of $\sigma_0 = 2e^2/h$) for interband transitions as a function of photon energy with magnetic field $B = 30$ T.

This is actually a reflection of the decreasing spacings in the LL spectrum plotted in Fig. 1(d). In particular, we plot the photon energies of the three kinds of allowed interband transitions $\Delta n = 0, \pm 2, \pm 4$ as a function of the level index in Fig. 3(d). As depicted in the figure, in low photon energy regime, only the lower LLs participate in the optical transitions. There is a large energy difference among the allowed transitions, which leads to separated peaks in the transition rate spectra [see Figs. 3(a) and 3(b)]. However, with the increase of photon energy, LLs with a high index are involved in the optical transitions. The difference of the nearest resonance energies corresponding to the allowed transitions becomes smaller and smaller and finally fades away [see Fig. 3(d)] with the increase of the level index arising from the smaller LL spacings depicted in Fig. 1(d). This contributes to merged peaks in the transition rate spectra in the high photon energy regime [see Figs. 3(a) and 3(b)]. Meanwhile, the transition rate shows strong anisotropy originating from the anisotropy of the LLs, i.e, the velocity operators and the wave functions. The $T_x^{vn,cn'}$ is two orders of magnitude larger than $T_y^{vn,cn'}$, resulting from the highly anisotropic velocity operators, which can also be inferred from the probability distributions plotted in Fig. 2.

With the help of the magneto-optical selection rule, now we can understand the magneto-absorption spectra more easily. Figure 3(e) presents the real part of the interband longitudinal magneto-optical conductivity as a function of photon energy under magnetic field $B = 30$ T. As shown in Fig. 3(e), the resonance frequency of the conductivity peak varies from the midinfrared to the far-infrared regime for $B = 30$ T. Of course, the resonance frequencies can be modulated by varying the magnetic fields. Further, the interband magneto-optical absorption spectra exhibit strong anisotropy inherited from the highly anisotropic transition rate spectra. The Reσ_{xx} (red line) is hundreds of times larger than Reσ_{yy} (blue line) resulting from the highly anisotropic band structure in the absence of magnetic field, i.e., the highly anisotropic velocities along different directions [see Eq. (11)]. Owing to the anisotropic magneto-optical selection rule, i.e., $\Delta n = 0, \pm 2$ ($\Delta n = \pm 2, \pm 4$) for linearly polarized light along the $x(y)$-direction, the conductivity peaks in Reσ_{xx} do not exactly coincide with those in Reσ_{yy}. In the low photon energy regime, we find well-resolved two-peak structures in Reσ_{xx} (Reσ_{yy}) corresponding to the transitions of $\Delta n = 0, \pm 2$ ($\Delta n = \pm 2, \pm 4$). With the increase of photon energy, LLs with high index are involved in the transition process. The differences of the nearest resonance energies corresponding to the allowed transitions ($\Delta n = 0, \pm 2, \pm 4$) become smaller and smaller. They finally vanish in the high photon energy regime [see Fig. 3(d)] resulting from the decreasing LL spacing plotted in Fig. 1(d). Therefore, although the selection rule has not changed, we can only find one conductivity peak in both Reσ_{xx} and Reσ_{yy} in the high photon energy regime. Quantitatively, the first conductivity peak in Reσ_{xx} is one order of magnitude larger than the others indicating a strong absorption from E_{v0} to E_{c0}. Other conductivity peaks in Reσ_{xx} contributed to by $\Delta n = 0$ are of the same order to those contributed to by $\Delta n = \pm 2$. In contrast, the conductivity peaks in Reσ_{yy} contributed to by $\Delta n = \pm 4$ are much smaller than those contributed to by $\Delta n = \pm 2$, which is also in line with the

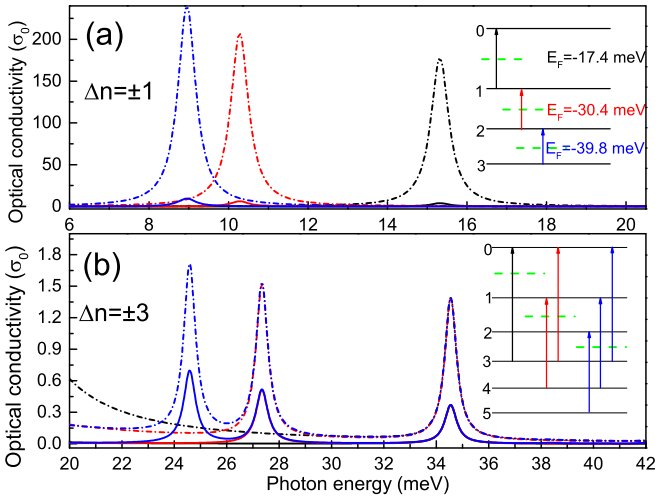

FIG. 4. The real part of the longitudinal magneto-optical conductivity as a function of the photon energy under magnetic field $B = 30$ T for intraband transitions of (a) $\Delta n = \pm 1$ and (b) $\Delta n = \pm 3$, respectively. The dash-dotted (solid) lines denote the results for polarized light along the $x(y)$-direction. The insets depict the transitions between the nearest LLs for transitions with filling factor $\nu = 1$ to 3. The color of the arrows is the same as that of the corresponding conductivity peaks.

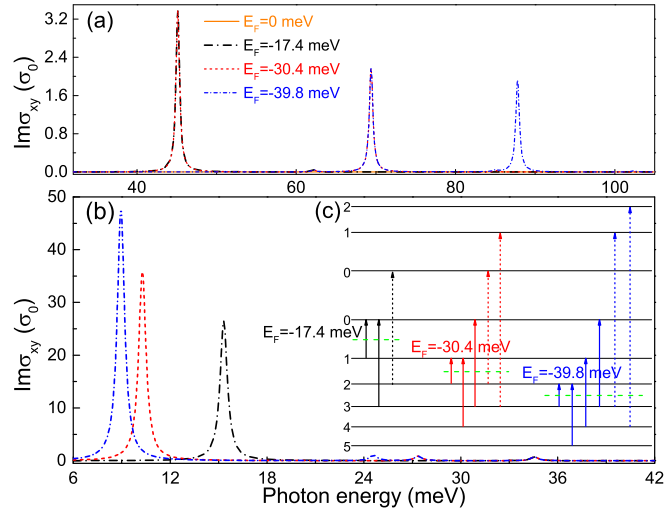

FIG. 5. The imaginary part of the Hall magneto-optical conductivity σ_{xy} as a function of photon energy under magnetic field $B = 30$ T for (a) interband and (b) intraband transitions. The inset (c) depicts the transitions contributing to the σ_{xy} with filling factor $\nu = 1$ to 3. The dash (solid) arrows denote the interband (intraband) transitions. The colors of the arrows are the same as that of the corresponding conductivity peaks.

transition rates shown in Fig. 3(b). Hence, Reσ_{yy} is dominated by the transition of $\Delta n = \pm 2$.

Next, we turn to discuss the intraband transitions. Figure 4 presents the real part of the longitudinal magneto-optical conductivity as a function of the photon energy under magnetic field $B = 30$ T for intraband transitions with filling factor $\nu = 1$ to 3. The dash-dotted (solid) lines denote the results for linearly polarized light along the $x(y)$-direction. In both Reσ_{xx} and Reσ_{yy}, the intraband transitions occur when the level index changes as $\Delta n = \pm 1, \pm 3$, contributing to two groups of absorption peaks. This indicates that the magneto-optical selection rule of intraband transitions is independent of the direction of polarization of light, i.e., isotropic selection rules. This is the same as the magneto-optical selection rules for intraband transitions in black phosphorus thin films [32]. All the absorption peaks occur at the terahertz (THz) frequencies. We schematically depicted the selection rules in the insets as the filling factor ν varying from 1 to 3. The color of the arrows in the insets is the same as that of the corresponding conductivity peaks. Although the selection rule is isotropic, the magneto-optical conductivity is still highly anisotropic. Reσ_{xx} is one order of magnitude larger than Reσ_{yy} because of the anisotropic velocity operator arising from the anisotropic dispersion at zero magnetic field. For a certain Fermi level, the conductivity in both Reσ_{xx} and Reσ_{yy} contributed to by the transition of $\Delta n = \pm 3$ is much smaller than that contributed by $\Delta n = \pm 1$. Therefore, the intraband conductivity is dominated by the dipole-type transitions ($\Delta n = \pm 1$). Under a fixed magnetic field, the resonant frequencies for the transitions of both $\Delta n = \pm 1$ and $\Delta n = \pm 3$ are red-shifted with the increase of filling factor (doping), which is a direct reflection of the decreasing LL spacings [see Fig. 1(d)]. The red-shift for the transitions of $\Delta n = \pm 3$ results in three-peak structures in the magneto-optical conductivity, which is more similar to the multipeak structures in graphene [38,45,46] and silicene [39] rather than the single peak structure in conventional semiconductors [44]. Moreover, the red-shift decreases with the filling factor which can be understood from Eq. (8). Further, we would like to point out that the interband and intraband magneto-optical conductivities reported here can be directly measured through the infrared spectroscopy [24,25] or the magneto-absorption experiments [26].

After discussing the longitudinal magneto-optical conductivities, i.e., σ_{xx} and σ_{yy}, now we consider the Hall magneto-optical conductivity σ_{xy}. Figure 5 presents the imaginary (absorption) part of the Hall magneto-optical conductivity as a function of photon energy under magnetic field $B = 30$ T for Fig. 5(a) interband and Fig. 5(b) intraband transitions. For interband transitions, owing to the anisotropic selection rules in the longitudinal magneto-optical conductivity spectra, the magneto-optical transition selection rule for Hall conductivity Imσ_{xy} is $\Delta n = \pm 2$. Surprisingly, for pristine sample, i.e., $E_F = 0$, the interband Imσ_{xy} is zero in all photon energy regimes [see the solid orange line in Fig. 5(a)]. The reason originates from the constrain of the chiral symmetry. Generally, for a two-band model preserving the chiral symmetry, the Hamiltonian H of the system satisfies $\sigma_z H \sigma_z^{-1} = -H$, where σ_z is the Pauli matrix [47]. Obviously, the chiral symmetry is preserved in our system because both Hamiltonians (1) and (4) fulfill the definition of the chiral symmetry. The chiral symmetry has a direct constrain on the eigenstate of the system. Namely, if ψ is an eigenstate of the Hamiltonian corresponding to eigenvalue E, then $\sigma_z \psi$ is the eigenstate of the Hamiltonian corresponding to eigenvalue $-E$ [47]. In view of this, we find the Hall magneto-optical conductivity contributed by $\Delta n = 2$ cancels that

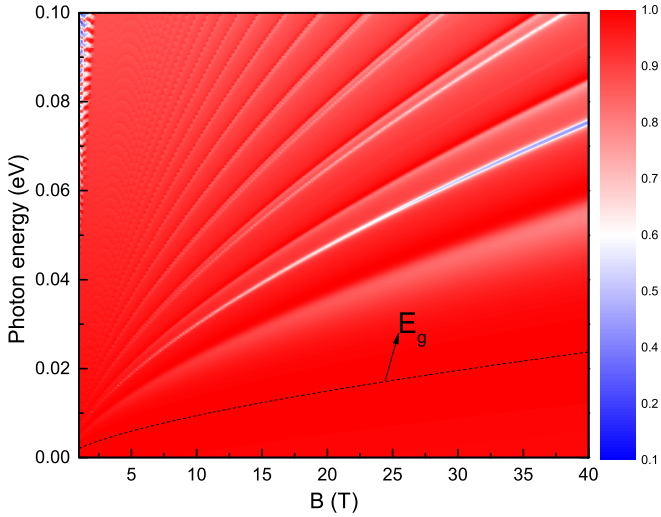

FIG. 6. Contour plot of the linear dichroism for interband transition as functions of photon energy and magnetic field. The black dashed line is the band gap of LL spectrum, which corresponds to the resonance energy of the perfect linear dichroism.

contributed from $\Delta n = -2$, leading to zero interband $\mathrm{Im}\sigma_{xy}$ in the pristine sample. We presented a detailed proof in the Appendix.

To obtain finite interband $\mathrm{Im}\sigma_{xy}$, we should focus on the electron or hole-doped sample. Taking the hole-doped sample with filling factor $\nu = 1$ as an example, the transition from $n_v = 0$ to $n_c' = 2$ is missing because the $n_v = 0$ LL is empty in this case, and only the transition from $n_v = 2$ to $n_c' = 0$ is preserved according to the transition rules $\Delta n = \pm 2$ [see the black dashed arrow in Fig. 5(c)]. Therefore, there is one conductivity peak in $\mathrm{Im}\sigma_{xy}$ indicating an absorption from E_{v2} to E_{c0} [see the black line in Fig. 5(a)]. Next, for the filling factor $\nu = 2$, only the transitions from $n_v = 2$ (3) to $n_c' = 0$ (1) are preserved [see the red dashed arrows in Fig. 5(c)], contributing to two absorption peaks in $\mathrm{Im}\sigma_{xy}$ [see the red line in Fig. 5(a)]. Similar conclusions can be drawn for the filling factor $\nu = 3$. For intraband transitions, Fig. 5(b) shows the intraband $\mathrm{Im}\sigma_{xy}$ as a function of photon energy for the hole-doped sample with filling factor $\nu = 1$ to 3. The selection rule in this case is also $\Delta n = \pm 1, \pm 3$ due to the isotropic selection rules in the intraband longitudinal magneto-optical conductivities [see the solid arrows in Fig. 5(c)]. As shown in Fig. 5(b), similar to the intraband longitudinal magneto-optical conductivities ($\mathrm{Re}\sigma_{xx}$ and $\mathrm{Re}\sigma_{yy}$), the intraband $\mathrm{Im}\sigma_{xy}$ is also dominated by the dipole transitions ($\Delta n = \pm 1$). The conductivity peaks in intraband $\mathrm{Im}\sigma_{xy}$ are also red-shifted with the increasing of the filling factor due to the deceasing LL spacings, which can be directly inferred from Eq. (8).

As discussed above, both the interband and intraband magneto-optical absorption spectra are highly anisotropic, which will result in a strong linear dichroism [48–50]. We define a dimensionless parameter $I = (\mathrm{Re}\sigma_{xx} - \mathrm{Re}\sigma_{yy})/(\mathrm{Re}\sigma_{xx} + \mathrm{Re}\sigma_{yy})$ to indicate the linear dichroism quantitatively [48]. Figure 6 presents a contour plot of the linear dichroism as a function of the photon energy and the magnetic field for the interband transitions. From the figure, we find that I is larger than 0.8 within most photon energies and magnetic fields because $\mathrm{Re}\sigma_{xx}$ is always dozens of times larger than $\mathrm{Re}\sigma_{yy}$. In principle, owing to the anisotropic selection rules, there should be a perfect linear dichroism for the photon energy corresponding to the transition of $\Delta n = 0$ ($\Delta n = \pm 4$) which is only allowed in $\mathrm{Re}\sigma_{xx}$ ($\mathrm{Re}\sigma_{yy}$). However, the differences of the resonance photon energy between the transitions $\Delta n = 0$ and $\Delta n = \pm 4$ are quenched in the high photon energy regime [see Fig. 3(d)] where the perfect linear dichroism is destroyed. Fortunately, the perfect linear dichroism survives in the low photon energy regime, where I is always 1 resulting from the transition from E_{v0} to E_{c0}, which only can be excited by linearly polarized along the x-direction. Importantly, the resonance energy of the perfect linear dichroism is exactly the band gap of the LL spectrum, which can be effectively modulated by the magnetic field (see the black dashed line). Therefore, we can realize a perfect linear dichroism in 2D semi-Dirac materials with a magnetic field tunable wavelength by using the transition from E_{v0} to E_{c0}, which is important to design new magneto-optical devices. There is also a strong linear dichroism for the intraband transition of $\Delta n = \pm 1$. It is similar to that of the interband transition in the high photon energy regime, and we do not present it here.

IV. SUMMARY

We examined the LLs and magneto-optical absorption properties of a 2D semi-Dirac electron system based on an effective $\boldsymbol{k} \cdot \boldsymbol{p}$ Hamiltonian and linear-response theory. We found that the LLs of the 2D semi-Dirac electron system can be understood as a hybridization of those of the Schrödinger and Dirac electron but with new features. By using the Kubo formula, we found that the selection rules for interband magneto-optical transitions are anisotropic with $\Delta n = 0, \pm 2$ ($\Delta n = \pm 2, \pm 4$) for linearly polarized light along the $x(y)$ -direction. Whereas, the selection rules for intraband magneto-optical transitions are $\Delta n = \pm 1, \pm 3$ regardless of the polarization direction of light. For the interband (intraband) transition, the optical conductivity for linearly polarized light along the x-direction is two (one) orders of magnitude larger than that along the y-direction. The highly anisotropic magneto-optical absorption spectra clearly reflect the structure of the LLs and result in strong linear dichroism. The interband transition from E_{v0} to E_{c0} can realize a perfect linear dichroism with a magnetic-field-tunable wavelength. The magneto-absorption spectra occur at the infrared frequency and can be detected directly by the infrared spectroscopy [24–26]. Our results shed light on the magneto-optical properties of the 2D semi-Dirac electron systems and pave the way to design magneto-optical devices based on it.

Note added. After more than one month of our submission, a similar work posted on arXiv also studied the magneto-optical properties of semi-Dirac electron system [51].

ACKNOWLEDGMENTS

This work was supported by the National Natural Science Foundation of China (Grants No. 11804092 and

No. 11774085), Project funded by China Postdoctoral Science Foundation (Grants No. BX20180097 and No. 2019M652777), and Hunan Provincial Natural Science Foundation of China (Grant No. 2019JJ40187).

APPENDIX

In this Appendix, we discuss the effect of chiral symmetry on the Hall magneto-optical conductivity. In general, for a two-band model preserving the chiral symmetry, the Hamiltonian H of the system satisfies $\sigma_z H \sigma_z^{-1} = -H$, where σ_z is the Pauli matrix [47]. Obviously, the chiral symmetry is preserved in our system because both Hamiltonians (1) and (4) fulfill the definition of the chiral symmetry. A direct consequence of the chiral symmetry is that if ψ is an eigenstate of the Hamiltonian corresponding to energy E, then $\sigma_z\psi$ is the eigenstate of the Hamiltonian corresponding to energy $-E$. Therefore, assuming that the eigenstate of Hamiltonian (4) corresponds to the Landau level E_{cn} in the conduction band is

$$|\psi_n^c\rangle = \begin{pmatrix} |f_n\rangle \\ |g_n\rangle \end{pmatrix}. \tag{A1}$$

Then, according to the chiral symmetry, the wave function of the Landau level $E_{vn} = -E_{cn}$ in the valence band is

$$|\psi_n^v\rangle = \sigma_z|\psi_n^c\rangle = \begin{pmatrix} |f_n\rangle \\ -|g_n\rangle \end{pmatrix}. \tag{A2}$$

From the numerical calculations, we know that the selection rule for interband Hall magneto-optical conductivity is $\Delta n = \pm 2$. Using Eqs. (A1) to (A2) and incorporating with the velocity matrix in Eq. (11), we obtain the matrix elements for the interband transition $\Delta n = \pm 2$ as

$$\langle\psi_{n+2}^v|v_x|\psi_n^c\rangle = -i[\langle f_{n+2}|v_F|g_n\rangle + \langle g_{n+2}|v_F|f_n\rangle], \tag{A3}$$

$$\langle\psi_n^v|v_x|\psi_{n+2}^c\rangle = -i[\langle f_n|v_F|g_{n+2}\rangle + \langle g_n|v_F|f_{n+2}\rangle], \tag{A4}$$

$$\langle\psi_n^c|v_y|\psi_{n+2}^v\rangle = i[\langle f_n|v_{y0}|g_{n+2}\rangle - \langle g_n|v_{y0}|f_{n+2}\rangle], \tag{A5}$$

$$\langle\psi_{n+2}^c|v_y|\psi_n^v\rangle = i[\langle f_{n+2}|v_{y0}|g_n\rangle - \langle g_{n+2}|v_{y0}|f_n\rangle], \tag{A6}$$

where $v_{y0} = v_0(\hat{a}^\dagger - \hat{a})$. Further, we obtain the matrix elements of the velocity operators for interband transitions with $\Delta n = \pm 2$ as

$$\begin{aligned} P_{\Delta n=2} &= \langle\psi_{n+2}^v|v_x|\psi_n^c\rangle\langle\psi_n^c|v_y|\psi_{n+2}^v\rangle \\ &= [\langle f_{n+2}|v_F|g_n\rangle + \langle g_{n+2}|v_F|f_n\rangle] \\ &\quad \times [\langle f_n|v_{y0}|g_{n+2}\rangle - \langle g_n|v_{y0}|f_{n+2}\rangle], \end{aligned} \tag{A7}$$

$$\begin{aligned} P_{\Delta n=-2} &= \langle\psi_n^v|v_x|\psi_{n+2}^c\rangle\langle\psi_{n+2}^c|v_y|\psi_n^v\rangle \\ &= [\langle f_n|v_F|g_{n+2}\rangle + \langle g_n|v_F|f_{n+2}\rangle] \\ &\quad \times [\langle f_{n+2}|v_{y0}|g_n\rangle - \langle g_{n+2}|v_{y0}|f_n\rangle]. \end{aligned} \tag{A8}$$

According to Eq. (15) and combining with the selection rules, the interband $\mathrm{Im}\sigma_{xy}$ is determined by $\mathrm{Im}[P_{\Delta n=2} + P_{\Delta n=-2}]$. However, according to Eqs. (A7) and (A8), we have $(P_{\Delta n=-2})^* = P_{\Delta n=2}$, leading to $\mathrm{Im}[P_{\Delta n=2} + P_{\Delta n=-2}] = 0$. Therefore, the interband $\mathrm{Im}\sigma_{xy}$ contributed by the transitions of $\Delta n = 2$ and $\Delta n = -2$ cancel each other out, leading to the zero interband Hall magneto-optical conductivity in pristine samples.

[1] A. H. Castro Neto, F. Guinea, N. M. R. Peres, K. S. Novoselov, and A. K. Geim, Rev. Mod. Phys. **81**, 109 (2009).
[2] N. P. Armitage, E. J. Mele, and A. Vishwanath, Rev. Mod. Phys. **90**, 015001 (2018).
[3] P. Dietl, F. Piéchon, and G. Montambaux, Phys. Rev. Lett. **100**, 236405 (2008).
[4] G. Montambaux, F. Piéchon, J.-N. Fuchs, and M. O. Goerbig, Phys. Rev. B **80**, 153412 (2009).
[5] S. Banerjee, R. R. P. Singh, V. Pardo, and W. E. Pickett, Phys. Rev. Lett. **103**, 016402 (2009).
[6] V. Pardo and W. E. Pickett, Phys. Rev. Lett. **102**, 166803 (2009).
[7] H. Huang, Z. Liu, H. Zhang, W. Duan, and D. Vanderbilt, Phys. Rev. B **92**, 161115(R) (2015).
[8] S. S. Baik, K. S. Kim, Y. Yi, and H. J. Choi, Nano Lett. **15**, 7788 (2015).
[9] Q. Liu, X. Zhang, L. B. Abdalla, A. Fazzio, and A. Zunger, Nano Lett. **15**, 1222 (2015).
[10] B. Ghosh, B. Singh, R. Prasad, and A. Agarwal, Phys. Rev. B **94**, 205426 (2016).
[11] H. Doh and H. J. Choi, 2D Mater. **4**, 025071 (2017).
[12] C. Wang, Q. Xia, Y. Nie, and G. Guo, J. Appl. Phys. **117**, 124302 (2015).
[13] J. Kim, S. S. Baik, S. H. Ryu, Y. Sohn, S. Park, B. G. Park, J. Denlinger, Y. Yi, H. J. Choi, and K. S. Kim, Science **349**, 723 (2015).
[14] T. Makino, Y. Katagiri, C. Ohata, K. Nomura, and J. Haruyama, RSC Adv. **7**, 23427 (2017).
[15] J. Jang, S. Ahn, and H. Min, 2D Mater. **6**, 025029 (2019).
[16] J. P. Carbotte, K. R. Bryenton, and E. J. Nicol, Phys. Rev. B **99**, 115406 (2019).
[17] S. Banerjee and W. E. Pickett, Phys. Rev. B **86**, 075124 (2012).
[18] F. Zhai and J. Wang, J. Appl. Phys. **116**, 063704 (2014).
[19] W. Chen, X. Zhu, X. Zhou, and G. Zhou, Phys. Rev. B **103**, 125429 (2021).
[20] F. Stern and W. E. Howard, Phys. Rev. **163**, 816 (1967).
[21] K. von Klitzing, Rev. Mod. Phys. **58**, 519 (1986).
[22] K. S. Novoselov, A. K. Geim, S. V. Morozov, D. Jiang, M. I. Katsnelson, I. V. Grigorieva, S. V. Dubonos, and A. A. Firsov, Nature **438**, 197 (2005).
[23] Y. Zhang, Y.-W. Tan, H. L. Stormer, and P. Kim, Nature **438**, 201 (2005).
[24] M. L. Sadowski, G. Martinez, M. Potemski, C. Berger, and W. A. de Heer, Phys. Rev. Lett. **97**, 266405 (2006).
[25] Z. Jiang, E. A. Henriksen, L. C. Tung, Y.-J. Wang, M. E. Schwartz, M. Y. Han, P. Kim, and H. L. Stormer, Phys. Rev. Lett. **98**, 197403 (2007).
[26] I. Crassee, J. Levallois, A. L. Walter, M. Ostler, A. Bostwick, E. Rotenberg, T. Seyller, D. Van Der Marel, and A. B. Kuzmenko, Nat. Phys. **7**, 48 (2011).

[27] P. Cheng, C. Song, T. Zhang, Y. Zhang, Y. Wang, J.-F. Jia, J. Wang, Y. Wang, B.-F. Zhu, X. Chen, X. Ma, K. He, L. Wang, X. Dai, Z. Fang, X. Xie, X.-L. Qi, C.-X. Liu, S.-C. Zhang, and Q.-K. Xue, Phys. Rev. Lett. **105**, 076801 (2010).
[28] T. Hanaguri, K. Igarashi, M. Kawamura, H. Takagi, and T. Sasagawa, Phys. Rev. B **82**, 081305(R) (2010).
[29] L. Li, F. Yang, G. J. Ye, Z. Zhang, Z. Zhu, W. Lou, X. Zhou, L. Li, K. Watanabe, T. Taniguchi, K. Chang, Y. Wang, X. Hui Chen, and Y. Zhang, Nat. Nanotech. **11**, 593 (2016).
[30] A. M. Witowski, M. Orlita, R. Stepniewski, A. Wysmolek, J. M. Baranowski, W. Strupinski, C. Faugeras, G. Martinez, and M. Potemski, Phys. Rev. B **82**, 165305 (2010).
[31] V. P. Gusynin, S. G. Sharapov, and J. P. Carbotte, New J. Phys. **11**, 095013 (2009).
[32] X. Zhou, W.-K. Lou, F. Zhai, and K. Chang, Phys. Rev. B **92**, 165405 (2015).
[33] X. Y. Zhou, R. Zhang, J. P. Sun, Y. L. Zou, D. Zhang, W. K. Lou, F. Cheng, G. H. Zhou, F. Zhai, and K. Chang, Sci. Rep. **5**, 12295 (2015).
[34] X. Zhou, W.-K. Lou, D. Zhang, F. Cheng, G. Zhou, and K. Chang, Phys. Rev. B **95**, 045408 (2017).
[35] Y. Jiang, R. Roldán, F. Guinea, and T. Low, Phys. Rev. B **92**, 085408 (2015).
[36] G. D. Smith, *Numerical Solutions of Partial Differential Equations: Finite Difference Methods*, 2nd ed., (Oxford Univ. Press, Oxford, 1978).
[37] T. Ando and Y. Uemura, J. Phys. Soc. Jpn. **36**, 959 (1974).
[38] M. Koshino and T. Ando, Phys. Rev. B **77**, 115313 (2008).
[39] C. J. Tabert and E. J. Nicol, Phys. Rev. Lett. **110**, 197402 (2013).
[40] Z. Li and J. P. Carbotte, Phys. Rev. B **88**, 045414 (2013).
[41] K. Esfarjani, H. R. Glyde, and V. Sa-yakanit, Phys. Rev. B **41**, 1042 (1990).
[42] J. Sári, M. O. Goerbig, and C. Tőke, Phys. Rev. B **92**, 035306 (2015).
[43] N. Zettili, *Quantum Mechanics: Concepts and Applications*, 2nd ed., (Wiley, New York, 2009).
[44] L. M. Roth, B. Lax, and S. Zwerdling, Phys. Rev. **114**, 90 (1959).
[45] L. A. Chizhova, J. Burgdörfer, and F. Libisch, Phys. Rev. B **92**, 125411 (2015).
[46] V. P. Gusynin, S. G. Sharapov, and J. P. Carbotte, Phys. Rev. Lett. **98**, 157402 (2007).
[47] T. O. Wehling, M. I. Katsnelson, and A. I. Lichtenstein, Chem. Phys. Lett. **476**, 125 (2009).
[48] C. Bao, H. Zhang, T. Zhang, X. Wu, L. Luo, S. Zhou, Q. Li, Y. Hou, W. Yao, L. Liu, P. Yu, J. Li, W. Duan, H. Yao, Y. Wang, and S. Zhou, Phys. Rev. Lett. **126**, 206804 (2021).
[49] H. Bentmann, H. Maaß, E. E. Krasovskii, T. R. F. Peixoto, C. Seibel, M. Leandersson, T. Balasubramanian, and F. Reinert, Phys. Rev. Lett. **119**, 106401 (2017).
[50] Ch. Roth, F. U. Hillebrecht, H. B. Rose, and E. Kisker, Phys. Rev. Lett. **70**, 3479 (1993).
[51] P. Sinha, S. Murakami, and S. Basu, arXiv:2110.12670.